ORIGINAL ARTICLE

New Implementation of Spin-orbit Coupling Calculation on Multi-configuration Electron Correlation Theory

Qianlong Zhou[1*] | **Bingbing Suo**[1*]

[1]Shaanxi Key Laboratory for Theoretical Physics Frontiers, Institute of Modern Physics, Northwest University, Xi'an, Shaanxi 710027, P.R. China

Correspondence
Bingbing Suo PhD, Institute of Modern Physics, Northwest University, Xi'an, Shaanxi, 710127, P.R. China
Email: Bingbing Suo

Funding information
National Key R&D Program of China, Grant/Award Number: 2017YFB0203402, 2017YFB0203404; National Natural Science Foundation of China, Grant/Award Number: 21673174, 21873077

For treating both relativistic effect and electron correlation, the spin-free exact two-component and spin-dependent first-order Douglas-Kroll-Hess (sf-X2C-so-DKH1) Hamiltonian and the state-interaction (SI) method are combined to calculate the spin-orbit coupling (SOC) on multi-configuration electron correlation theory. Here, SOC is evaluated via SI among the spin-free states from the complete active space self-consistent field (CASSCF) calculation, and the dynamic electron correlation could be reckoned via the high-level multi-reference electron correlation method. Work equations to evaluate SOC matrix elements over spin-adapted Gelfand states in the framework of the graphic unitary group approach (GUGA) are presented. Benchmark calculations have verified the validity of the present implementation. As a pilot application, the internally contracted MRCI (icMRCI) with the inclusion of SOC calculation produces the reasonable equilibrium bond length and the harmonic vibrational frequency of the ground state of AuO, as well as the transition energy of $X^2\Pi_{3/2} \leftarrow^2 \Pi_{1/2}$.

KEYWORDS
electron structure theory, relativistic effect, electron correlation, spin-orbit coupling, graphical unitary group approach

Abbreviations: sf-X2C-so-DKH1, spin-free exact two-component and spin-dependent first order Douglas-Kroll-Hess; SI, state-interaction; SOC, spin-orbit coupling; GUGA, graphical unitary group approach.

1 | INTRODUCTION

Precise molecular electronic structure calculation asks for treating both electron correlation and relativistic effect elaborately.[1, 2] Electron correlation problem arises from the one-electron approximation for solving many-body Schrödinger or Dirac equation, which neglects the spontaneous interaction of electrons. Thus, there is a small energy difference (so-called electron correlation energy) between the calculated energy and the exact energy (full configuration interaction result) for a given finite basis set. Enormous methods have been developed to treat the electron correlation,[1] in which the two-step multi-configuration electronic correlation theory has proven to be successful in studying the strongly correlated molecules.[3] In such methods, the electron correlation is usually divided into the static and the dynamic correlation. The static correlation is first calculated by multi-configuration self-consistent-field (MCSCF) theory, then multi-reference electron correlation calculations as multi-reference configuration interaction (MRCI)[4, 5, 6] or multi-reference second-order perturbation theory (MRPT2)[7, 8, 9, 10] are performed to handle the dynamic correlation.

Relativistic effect relates to many physical phenomena as zero-field splitting, spin-forbidden reactions, and intersystem crossing, *etc.*[2] In the past twenty years, an important progress in dealing with the relativistic effect in the molecular electronic structure theory is the introduction of exact two-component (X2C) relativistic Hamiltonian.[11, 12, 13, 14] If the relativistic effect is not too strong, it is advantageous to separate the relativistic Hamiltonian into spin-free and spin-dependent terms.[15, 16] The spin-free term handles the scalar relativistic effect and have been treated variationally to infinite order by the spin-free X2C (sf-X2C) Hamiltonian. The spin-dependent term that describes the spin-orbit coupling (SOC), could truncate to finite order as the first-order Douglas-Kroll-Hess (so-DKH1) Hamiltonian.[16] The sf-X2C Hamiltonian can be implemented easily in the existing quantum chemistry package by slightly modifying one-electron term, and thus self-consistent-field (SCF) calculation have included the scalar relativistic effect naturally. On the contrary, calculating the spin-dependent term has many choices and requires more effort. One may include SOC in the SCF calculation by using complex-valued spinors. One may only use sf-X2C Hamiltonian in SCF but dealing with SOC in the electron correlation calculation. The later scheme has been implemented in the Beijing Density Functional (BDF) package,[17, 18, 19, 20] based on the equation-of-motion coupled-cluster (EOM-CC) theory[21] and time-dependent density functional (TDDFT) theory.[22] However, those implementations only focus on the single-reference correlation methods, limiting its usage on the weakly correlated systems. For the strongly correlated molecules, only the multi-configuration calculation is reliable. Therefore, it is highly desired to implement the sf-X2C+so-DKH1 Hamiltonian on multi-configuration calculation.

We have developed an multi-reference electron correlation package named Xi'an-CI,[23, 24, 25, 26, 27] which has been interfaced with BDF. Xi'an-CI supports uncontracted and internally contracted MRCI calculations,[26, 27] as well as several MRPT2 algorithms as multi-state n-electron valence state second order perturbation theory (MS-NEVPT2)[27] and static-dynamic-static second order perturbation theory (SDS-PT2).[10] It is interesting to go further to deal with the relativistic effect. For calculating the Hamiltonian matrix elements, Xi'an-CI uses the graphical unitary group approach (GUGA)[28, 29, 30, 31, 32], which expands the configuration interaction (CI) space on Gelfand states[33]. Unlike the Slater Determinant that is the eigenfunction of $\hat{S}_z$, Gelfand state is the eigenfunction of the $\hat{S}^2$ operator. However, calculation of the Hamiltonian matrix element on the Gelfand state is not as direct as using Slater Determinant. Herein, we would first present an algorithm to calculate the SOC matrix element based on GUGA and give all work equations. Moreover, the sf-X2C-so-DKH1 Hamiltonian and the state interaction (SI) method are used to consider SOC on the level of multi-configuration electron correlation theory. The present work provides a new choice for treating the electron correlation and the relativistic effect in the molecular electronic structure calculation.

This work organizes as follows. In Sec. II, we first introduce the SI approach to calculate SOC, then work equations

for evaluating the SOC matrix elements on Gelfand states are presented. In Sec. III, benchmark calculations are performed to check the validity of our implementation. The concluding remarks and perspectives will be given in Sec. IV.

2 | THEORY

2.1 | The state interaction approach

Starting from the spin-separated sf-X2C+so-DKH1 Hamiltonian in the second-quantized form,[15, 16]

$$H = H_{sf} + H_{so} \tag{1}$$

here, H_{sf} and H_{so} are the spin-free and spin-dependent Hamiltonian as,

$$H_{sf} = \sum_{pq} [\mathbf{h}^{X2C}_{+,sf}]_{pq} a^{\dagger}_{p} a_q + \frac{1}{2} \sum_{pqrs} (pr|qs) a^{\dagger}_{p} a^{\dagger}_{q} a_s a_r \tag{2}$$

$$\begin{aligned} H_{so} &= \sum_{pq} [\mathbf{H}_{so,1e}]_{pq} a^{\dagger}_{p} a_q \\ &= \sum_{pq} \left([\mathbf{h}_{so,1e}]_{pq} + [\mathbf{F}_{so,1e}]_{pq} \right) a^{\dagger}_{p} a_q \end{aligned} \tag{3}$$

where p, q, r, and s are the spin orbitals, $(pr|qs)$ are two-electron integrals written in Mulliken's notation, $[\mathbf{h}^{X2C}_{+,sf}]_{pq}$ are spin-free one-electron integrals. The $[\mathbf{H}_{so,1e}]_{pq}$ are effective one-electron SOC integrals that are summation of one-electron SOC integral $[\mathbf{h}_{so,1e}]_{pq}$ and mean-field integral $[\mathbf{F}_{so,1e}]_{pq}$, respectively (see section 1 in Supporting Information). The mean-field SOC integral is used to handle the two-electron SOC interaction. Thus, we do not need to consider two-electron SOC term explicitly. The detailed discussion for deducing the sf-X2C-so-DKH1 Hamiltonian could be found in Ref. [15] and [16]. A simple introduction to sf-X2C-so-DKH1 Hamiltonian is also presented in section 1 of supporting information for clarity.

In the SI approach, the Hamiltonian matrix in a configuration interaction space expanded by a set of electronic states $\{\Psi_I(S), I = 1, 2, \cdots, M\}$ is diagonalized,

$$H_{sf} |\Psi_I(S)\rangle = E_I |\Psi_I(S)\rangle \tag{4}$$

$$|\Psi_I(S)\rangle = \sum_{\mu} C_{\mu I} |\psi_\mu(S)\rangle \tag{5}$$

where $\Psi_I(S)$ is linear combination of configuration state functions $\psi_\mu(S), \mu = 1, 2, \cdots, NI$. S is the total spin of the state $\Psi_I(S)$. If GUGA is used, $\psi_\mu(S)$ is Gelfand state and is represented as the step vector,[28, 34, 31, 35]

$$|\psi_\mu(S)\rangle = |(d)S\rangle \tag{6}$$

$$= |(d_1, d_2, \cdots, d_n)S\rangle \tag{7}$$

where n is number of molecular orbitals. d_i $(i = 1, 2, \cdots, n)$ is a step on the orbital i. Because Ψ_I is the eigenstate of H_{sf}, the diagonal element of the Hamiltonian matrix is energy E_I and H_{so} only contributes to the off-diagonal element

as

$$\langle \Psi_I(S'M')|H|\Psi_J(SM)\rangle = \delta_{IJ}\delta_{S'S}E_I + \langle \Psi_I(S'M')|H_{so}|\Psi_J(SM)\rangle, \tag{8}$$

in which $M = S, S-1, \cdots, 1-S, -S$. $\Psi_I(SM)$ is introduced to distinguish the spin-component of a state $\Psi_I(S)$. $\Psi_I(S)$ can be obtained from multi-configuration electron correlation calculation such as complete active space self-consistent-field calculation (CASSCF), MRCI or MRPT2. In this work, the SOC matrix elements are evaluated over states from the CASSCF calculation.[36, 37] The diagonal element of Hamiltonian could be energies from CASSCF, or the higher level multi-reference electron correlation calculations as MRCI, MRPT2. The advantage of the present SI scheme is that the computational effort of SOC is small, and the higher-level methods have considered the dynamic electron correlation.

2.2 | The SOC matrix element over Gelfand states

The spin-orbit coupling Hamiltonian is written in form of second quantization as,

$$H_{SO} = \sum_{i\sigma,j\tau}\sum_{\gamma}(-1)^{\gamma}\langle i\sigma|\xi^{(1)}(r_1)l_{-\gamma}S_{\gamma}|j\tau\rangle E_{i\sigma,j\tau} \tag{9}$$

here, $i\sigma$ is the orthonormal spin orbital with $\sigma = \pm\frac{1}{2}$, $i = 1, 2, \cdots, n$, and $\gamma = 0, \pm 1$. The index σ is used to distinguish the spin-up and spin-down orbitals. $E_{i\sigma,j\tau}$ is the generator of U(2n) group,

$$E_{i\sigma,j\tau} = a^{\dagger}_{i\sigma}a_{j\tau} \tag{10}$$

in which $a^{\dagger}_{i\sigma}$ and $a_{j\tau}$ are the creation operator and the annihilation operator, respectively. The $\langle i\sigma|\xi^{(1)}(r_1)l_{-\gamma}S_{\gamma}|j\tau\rangle$ is a general form of the one-electron SOC integral which can be calculated from the Breit-Pauli Hamiltonian,[38, 39] or from so-DKH1 Hamiltonian.[15, 16, 21] In this work, we adopt the so-DKH1 Hamiltonian implemented in BDF (Eqn. 3).

The matrix element of the H_{so} operator over Gelfand states is written as

$$\begin{aligned}
&\langle (d)'S'M'|H_{so}|(d)SM\rangle \\
&= \sum_{i\sigma,j\tau}\sum_{\gamma}(-1)^{\gamma}\langle i|\xi^{(1)}(r_1)l_{-\gamma}|j\rangle\langle\sigma|S_{\gamma}|\tau\rangle \\
&\qquad \cdot \langle (d)'S'M'|E_{i\sigma,j\tau}|(d)SM\rangle \qquad (11)\\
&= \sum_{i,j}\sum_{\gamma}(-1)^{\gamma}\langle i|\xi^{(1)}(r_1)l_{-\gamma}|j\rangle \\
&\qquad \cdot \langle (d)'S'M'|F^{(1)}_{\gamma}(i,j)|(d)SM\rangle \qquad (12)\\
&F^{(1)}_{\gamma}(i,j) = \sum_{\sigma,\tau}\langle\sigma|S_{\gamma}|\tau\rangle E_{i\sigma,j\tau} \qquad (13)
\end{aligned}$$

The term $\langle (d)'S'M'|F^{(1)}_{\gamma}(i,j)|(d)SM\rangle$ in equation 12 is the coupling coefficient that can be evaluated in terms of

the U(n+1) generator as,[40]

$$\begin{aligned}&\langle (d)'S'M'|F_{\gamma}^{(1)}(i,j)|(d)SM\rangle = \\ &(-1)^{S'-M'+S_{n+1}+1-\frac{1}{2}}\frac{1}{\sqrt{6}}\begin{pmatrix} S' & 1 & S \\ -M' & \gamma & M\end{pmatrix}\begin{Bmatrix} S' & S & 1 \\ \frac{1}{2} & \frac{1}{2} & S_{n+1}\end{Bmatrix}^{-1}\cdot \\ &\langle (d')_{n+1}S_{n+1}M_{n+1}|e_{i,n+1;n+1,j}+\frac{1}{2}E_{ij}|(d)_{n+1}S_{n+1}M_{n+1}\rangle\end{aligned} \tag{14}$$

in which the $E_{ij} = \sum_{\sigma} E_{i\sigma,j\sigma}$ is the generator of the U(n) group, and

$$e_{i,n+1;n+1,j} = E_{i,n+1}E_{n+1,j} - E_{ij} \tag{15}$$

From Eqn. 14 and the Wigner-Eckart Theorem (Eqn. 16),

$$\begin{aligned}&\langle (d)'S'M'|F_{\gamma}^{(1)}(i,j)|(d)SM\rangle \\ &= (-1)^{S'-M'}\begin{pmatrix} S' & 1 & S \\ -M' & \gamma & M\end{pmatrix}\langle (d)'S'||F^{(1)}(i,j)||(d)S\rangle\end{aligned} \tag{16}$$

the reduced matrix element is calculated as

$$\begin{aligned}&\langle (d)'S'||F^{(1)}(i,j)||(d)S\rangle \\ &= (-1)^{S_{n+1}+S-1/2}\frac{1}{\sqrt{6}}\begin{Bmatrix} S' & S & 1 \\ \frac{1}{2} & \frac{1}{2} & S_{n+1}\end{Bmatrix} \\ &\cdot\langle (d')_{n+1}S_{n+1}M_{n+1}|e_{i,n+1;n+1,j}+\frac{1}{2}E_{ij}|(d)_{n+1}S_{n+1}M_{n+1}\rangle\end{aligned} \tag{17}$$

Therefore, the SOC matrix elements can be calculated from the reduced matrix element as

$$\begin{aligned}&\langle (d)'S'M'|H_{SO}|(d)SM\rangle \\ &= \sum_{i,j}\sum_{\gamma}(-1)^{\gamma+S'-M'}\langle i|\xi^{(1)}(r_1)|j\rangle\begin{pmatrix} S' & 1 & S \\ -M' & \gamma & M\end{pmatrix} \\ &\cdot\langle (d)'S'||F^{(1)}(i,j)||(d)S\rangle\end{aligned} \tag{18}$$

The selection rule of the SOC matrix element is obtained from the triangular conditions of the 6j symbol,

$$S' - S = 0, \pm 1 \text{ but not } S' = S \neq 0 \tag{19}$$

This selection rules restrict the step vectors of Bra and Ket state on the $(n+1)$th orbital as,

$$S_{n+1} = \begin{cases} S+\frac{1}{2}, & S' = S, & d'_{n+1} = 1, d_{n+1} = 1 \\ S-\frac{1}{2}, & S' = S, & d'_{n+1} = 2, d_{n+1} = 2 \\ S+\frac{1}{2}, & S' = S+1, & d'_{n+1} = 2, d_{n+1} = 1 \\ S-\frac{1}{2}, & S' = S-1, & d'_{n+1} = 1, d_{n+1} = 2 \end{cases} \tag{20}$$

The coupling coefficient (Eqn. 14) can be calculated from

$$\begin{aligned} &\langle (d')_{n+1} S_{n+1} M_{n+1} | e_{i,n+1;n+1,j} + \frac{1}{2} E_{ij} | (d)_{n+1} S_{n+1} M_{n+1} \rangle \\ &= W^{(1)}(A^R, d'_i d_i) [\prod_{r=i+1}^{j-1} W^{(1)}(C', d'_r d_r)] W^{(1)}(B^L, d'_j d_j) \\ &\cdot [\prod_{r=j+1}^{n} W^{(1)}(C'', d'_r d_r)] W^{(1)}(D_{RL}, d'_{n+1} d_{n+1}) \end{aligned} \tag{21}$$

for $i < j$, and

$$\begin{aligned} &\langle (d')_{n+1} S_{n+1} M_{n+1} | e_{i,n+1;n+1,j} + \frac{1}{2} E_{ij} | (d)_{n+1} S_{n+1} M_{n+1} \rangle \\ &= W^{(1)}(A^L, d'_j d_j) [\prod_{r=j+1}^{i-1} W^{(1)}(C', d'_r d_r)] W^{(1)}(B^R, d'_i d_i) \\ &\cdot [\prod_{r=i+1}^{n} W^{(1)}(C'', d'_r d_r)] W^{(1)}(D_{RL}, d'_{n+1} d_{n+1}) \end{aligned} \tag{22}$$

for $i > j$. In the Eqn. 21 and 22, $W^{(1)}(A^R)$, $W^{(1)}(B^L)$, $W^{(1)}(A^L)$, $W^{(1)}(B^R)$, and $W^{(1)}(D_{RL})$ are so called segment factors in GUGA, [35] which are presented in Table S1 in SI. Only two types of factors, $D_{RL} - C'' - B^R - C' - A^L$ and $D_{RL} - C'' - B^R - C' - A^R$ need to be calculated. The factor $D_{RL}-$ lies on the dummy $(n+1)th$ orbital. Due to the Hamiltonian matrix is Hermit, only $S' = S$ and $S' = S-1$ are considered in calculation, which give rise to the segment factors $D_{RL}(11)-$ and $D_{RL}(12)-$. Eqn. 17, 18, 21, and 22 constitute all work equations in our approach to calculate the SOC matrix element.

3 | RESULTS AND DISCUSSION

Benchmark calculations were performed to check the validity of our implementation. In all calculations, the diagonal elements of Hamiltonian matrix were calculated on CASSCF or MRCI, while the off-diagonal elements (the SOC matrix elements) were evaluated over states from CASSCF. For the MRCI calculation, the Celani and Werner's internally contracted multi-reference configuration interaction with single and double excitations (CW-icMRCISD) in Xi'an-CI package was used.[41, 26, 27] The Pople correction (CW-icMRCISD+Q) was applied to correct the size-consistent error.[42] We use the same molecular orbitals for the different spin states to calculate the SOC integral, that is, all states with the different spin and spatial symmetries are optimized in the state-averaged CASSCF (SA-CASSCF) calculation with equal weights. The atomic natural orbital at the polarized valance triple zeta (ANO-TZVP) level of basis set developed by Roos *et. al.* are used in all calculations.[43] The reference calculations are performed by MOLCAS (Version 8.0),[44, 36] Molpro (Version 2015),[45, 46] and GAMESS (Version 2020-R1).[47, 37] with the same basis

set. Notice the relativistic Hamiltonian and methods used to consider SOC in other programs are different from those used in our approach. We will give detailed information in each benchmark calculation.

3.1 | SOC splitting of ^2P state of Halogen atoms

The ground state of the Halogen atom is ^2P with the configuration of np^5. The ^2P state splits into $^2P_{3/2}$ and $^2P_{1/2}$, and the splitting energy is always used as a prototype to check the SOC effect. Table 1 depicts the energy gap of $^2P_{3/2}$ and $^2P_{1/2}$ of Halogen atoms calculated with several different methods as well as the experimental data from NIST.[48] All of the first three calculations, BDF, MOLCAS, and Molpro are the SI calculations based on the CASSCF wave functions (denoted as CASSI). The active space is chosen as complete active space (4o, 7e). The SHCI result takes from Ref. [49], in which SOC was calculated on the heat bath configuration interaction with the stochastic perturbation (SHCI) method. The EOM-CC result takes from Ref. [21] that considers the SOC on equation-of-motion coupled-cluster (EOM-CC) theory. In all calculations, the sf-X2C is applied to consider the spin-free term. The so-DKH1 Hamiltonian is used in BDF, SHCI and EOM-CC for the SOC interaction. In MOLCAS and Molpro calculations, atomic mean field integrals (AMFI) and the Breit-Pauli operator are used to consider SOC, respectively.

TABLE 1 Spin-orbit splitting of $^2P_{3/2}$ and $^2P_{1/2}$ states of Halogen atoms

Atom	BDF	MOLCAS	Molpro	SHCI[a]	EOM-CC[b]	Expt.
F	405	405	404	399	398	404
Cl	829	828	840	866	876	882
Br	3434	3413	3454	3691	3648	3685
I	7032	6973	8444	7487	7754	7603

[a] Ref. [49], active spaces (100o, 17e) and (121o,17e) are used for Br and I, respectively. The active space (4o,7e) gives splitting energies 3428 and 7021 cm^{-1} for Br and I, respectively.

[b] Ref. [21]

As seen in Table 1, all calculations agree well with the experimental data from NIST, especially for the lightest atom F, where the absolute errors for the first three calculations are within 1 cm^{-1}. Errors increase with the enlarging of nuclear charge, indicating by the absolute errors have the order F<Cl<Br<I. The SHCI and EOM-CC calculations produce better results for the Br and I atoms than the three CASSI calculations. The reason is that the SOC interactions of Br and I are strong, and CASSI is insufficient to reproduce the SOC interaction at very high precision because of too small active space. The SHCI calculation that used much large active space, yields the splitting energies 3691 and 7487 cm^{-1} for Br and I, agreeing well with the data from NIST. The EOM-CC results are also fairly well for Br and I due to the excitation amplitudes are relaxed in the SOC calculation,[21] being equivalent to enlarge the active space. However, errors of CASSI for Br and I are within 12%, which is acceptable in considering CASSI is much cheaper than SHCI and EOM-CC.

Both BDF and MOLCAS underestimate the splitting energy of the I atom, while Molpro tends to overestimate it. Since all the first three calculations are CASSI, such difference arises from the different relativistic Hamiltonian in calculation. In BDF, the sf-X2C+so-DKH1 Hamiltonian is used, and the two-electron contribution is considered via a

mean-field approach, which is similar to the AMFI used in MOLCAS. However, Molpro applies the BP Hamiltonian and two-electron term is also invoked as the mean-field approach. Theoretically, sf-X2C-so-DKH1 is superior to the BP Hamiltonian because both scaler relativistic effect and SOC are considered more precisely, especially for the I atom.

3.2 | Excitation energies of $^3P_{1,2}$,$^1D_2$ and $^1S_0$ state of the group IVA atoms

Table 2 presents the excitation energies of the first four excited states of the group IVA elements. The spin-free ^3P state is three-fold degenerate. The ^1D state is five-fold degenerate. For preserving the spatial degeneracy of the spin-free states, we adopt the C_i point group in calculation, in which the ^1S and ^1D states have the A_g symmetry while the ^3P state appears in the A_u *irreps*. Thus, six roots (1 root for ^1S and 5 roots for ^1D) are considered in the A_g *irreps*, and three roots (^3P) are considered in the A_u *irreps*. Since dynamic correlation was important in calculating the excitation energies, CW-icMRCISD+Q were performed to calculate the spin-free states via the Xi'an-CI package. MOLCAS is used in the reference calculation, in which energies of spin-free states are calculated by multi-state complete active space second-order perturbation theory (MS-CASPT2), and SOC is evaluated by CASSI.

TABLE 2 Excitation energy of first four excited states of the group IVA atoms[a]

Atom	Method	$^3P_1$	$^3P_2$	$^1D_0$	$^1S_0$
C	MRCI	15	45	10552	22574
	CASPT2	15	45	10591	20959
	Expt.	16	43	10192	21645
Si	MRCI	66	193	6431	15941
	CASPT2	67	195	6747	14350
	Expt.	77	223	6298	15394
Ge	MRCI	493	1275	9580	17199
	CASPT2	488	1226	8830	18229
	Expt.	557	1609	7125	16376
Sn	MRCI	1454	3059	8807	17252
	CASPT2	1443	3057	9021	18045
	Expt.	1691	3427	8612	17162

[a] MRCI is CW-icMRCISD and SOC is considered as CASSI. CASPT2 is MS-CASPT2 and SOC is considered as CASSI. The active space is (4o, 6e).

The excitation energy of the $^3P_1$ and $^3P_2$ states is mainly determined by SOC splitting of the spin-free ^3P state, thus our calculation and MOLCAS yield similar results for excitation energies of the $^3P_1$ and $^3P_2$ states as illustrated in Table 2. Moreover, energy errors of the first two states are small for C and Si but are large for Ge and Sn. Similar to the result of the Halogen atoms, both our and MOLCAS calculations tend to underestimate the excitation energies of the $^3P_1$ and $^3P_2$ states of the relatively heavier atoms Ge and Sn.

As seen in Table 2, excitation energy errors of $^1D_0$ and $^1S_0$ are not as systematic as those of $^3P_{1,2}$. The $^1D_0$ and $^1S_0$ are not coupling directly due to the selection rule, but both of them are coupling weakly with the ^3P state. Due to zero-field splitting pushes the ground $^3P_0$ state to the lower energy, the calculated excitation energies of $^1D_0$ and $^1S_0$ should be mainly determined by the zero-field splitting of ^3P and energy levels of the spin-free ^1D and ^1S states. The energy differences between MRCI and CASPT2 mainly arise from the different excitation energies of spin-free states because the calculated zero-field splitting of the ^3P state are close in two methods. Although the absolute energy errors are different, both MRCI and CASPT2 yield quantitatively correct excitation energies of the $^1D_0$ and $^1S_0$ states.

3.3 | SOC between the $^1A_1$ and $^3B_1$ states of the XH_2 molecules

SOC between the $^1A_1$ and $^3B_1$ states of XH_2 (X=C, Si, Ge, Sn, and Pb) had been calculated by Fedorov and Gordon to exam the two-electron SOC (2e-SOC) contribution.[37] In the present work, we only calculate one-electron SOC interaction (1e-SOC) explicitly, and the 2e-SOC contribution is considered by the mean-field approximation in the one-electron SOC integrals (denoted as 1e+soMF). Therefore, it is interesting to compare the mean-field scheme with the algorithm that fully includes the 2e-SOC contribution. Table 3 presents the SOC matrix elements of $^3B_1 - ^1A_1$ of the XH_2 molecules calculated with BDF, MOLCAS, and GAMESS, in which GAMESS can calculate the 2e-SOC term explicitly on the CASSCF level of theory. MOLCAS uses AMFI to consider 2e-SOC. For comparison, we also performed the SOC calculation only considering the 1e-SOC in BDF and GAMESS, which are labelled as 1e and 1e-BP in table 3, respectively. Geometries of XH_2 in calculation are taken from Ref. [50].

TABLE 3 SOC matrix element between the $^1A_1$ and $^3B_1$ states of the XH_2 molecules

Molecule	1e[a]	1e+soMF[a]	AMFI[b]	1e-BP[c]	1e+2e-BP[c]
CH_2	17	10	9	17	9
SiH_2	47	37	37	48	37
GeH_2	292	261	258	326	280
SnH_2	675	630	626	742	685
PbH_2	2296	2207	2162	2242[d]	2140[d]

[a] 1e, BDF calculation with only 1e-SOC term. 1e+soMF, BDF calculation with 1e-SOC and mean-field 2e-SOC.

[b] AMFI, atomic mean-field integral approach calculated by MOLCAS.

[c] 1e-BP, GAMESS calculation with only 1e-SOC term. 1e+2e-BP, GAMESS calculation with 1e-SOC and full 2e-SOC. BP Hamiltonian was used.

[d] Ref. [37]. WTBS basis set.

As seen in Table 3, SOC matrix elements calculated from the mean-field approach are in line with results that fully include 2e-SOC contribution. For CH_2 and SiH_2, SOC matrix elements calculated by BDF and MOLCAS are close to results from GAMESS (full 2e-SOC). For heavier elements Ge, Sn, and Pb, the BDF results agree with MOLCAS within

tens of cm^{-1} but have large discrepancies with GAMESS. These large discrepancies are caused by the different SOC operators rather than the different methods in considering 2e-SOC, that is, the BP operator used in GAMESS that tends to give the stronger SOC interaction than the so-DHK1 Hamiltonian. Notice that the relative contribution of the 2e-SOC term is large in the full SOC matrix elements as CH_2 and SiH_2, thus 2e-SOC is more important in calculating the light elements. Since the mean-field approach is cheap and only introduces a small computational overhead in the SOC integral, thus it always should take into account 2e-SOC for system as pure organic molecules.

3.4 | Spectroscopic parameters of the $X^2\Pi_{3/2}$ and $^2\Pi_{1/2}$ states of AuO

There are many experimental and theoretical studies on the spectra of the AuO molecule.[51, 52, 53, 54, 55] The relativistic effect plays a significant role in determining the spectroscopic parameters of AuO. As a pilot application, potential energy curve of the $^2\Pi$ state of AuO is calculated by CW-icMRCISD+Q. Then, SOC is evaluated by CASSI. In the CW-icMRCISD+Q calculation, the active space is selected as the molecular orbital composed of the 2s, 2p orbital of O and 5d, 6s of Au. A larger active space made up of O 2p, 3p, and Au 5d, 6s is used in the SOC calculation. Besides, the $^4\Sigma^-$ state is included in the SOC calculation because benchmark indicates this state is coupling strongly with the $^2\Pi$ state.

As seen in Table 4, the ground $X^2\Pi_{3/2}$ state of AuO has the equilibrium bond length of 1.867 Å with the harmonic vibrational frequency of 633 cm^{-1}, being close to 1.861 Å and 624 cm^{-1} obtained via the CASPT2 calculation with the inclusion of SOC from O'Brien, Oberlink and Roos.[54] The first excited $^2\Pi_{1/2}$ state has a longer r_e of 1.887 Å and a smaller ω_e of 587 cm^{-1}, and the CASPT2 results are 1.886 Å and 597 cm^{-1}, respectively. The only experimental data for the equilibrium bond length of the $^2\Pi_{1/2}$ state is 1.917 ± 10Å from Ichino et al.[52]. However, the experimental r_e of $X^2\Pi_{1/2}$ is somehow controversial. Okabayashi and co-workers obtained $r_e = 1.8487$ Å by analysing the pure rotational spectrum of the ground $X^2\Pi_{3/2}$ state,[53] but O'Brien *et al.* got a longer bond length of 1.906 Å from resolving the near-infrared electronic spectrum.[51] Both CW-icMRCISD+Q and CASPT2 calculations support Okabayashi *et al.*'s result, that is, the ground state of AuO should has a short equilibrium bond length near 1.85 Å. Moreover, the vibrational frequency 633 cm^{-1} from our calculation is close to the newest experimental value 640 cm^{-1} from Xiang *et al.*[55] Although the CCSD(T) and internally contracted MRCI calculations from Ichino *et al.* gave $r_e = 1.907$ Å,[52] agreeing well with O'Brien's data,[51] these two calculations not only used effective core potential (ECP) to treat relativistic effect but also did not consider the SOC effect. On the contrary, both the CW-icMRCISD+Q and CASPT2 calculations used the full electron basis set and considered the relativistic effect elaborately, thus results should be more reliable. This conclusion is also supported by the calculated transition energy 1541 cm^{-1} of $X^2\Pi_{3/2} \longleftarrow^2 \Pi_{1/2}$, which is close to the value of 1440 ± 80 cm^{-1} estimated from the experimental photoelectron spectra.[52]

4 | CONCLUSION

SOC is calculated in the framework of multi-configuration electronic correlation theory. The work equations to evaluate SOC matrix elements over the Gelfand states in GUGA are presented. As the first implementation, the SI approach is utilized in which off-diagonal elements of the Hamiltonian matrix are SOC among the spin-free states calculated on the CASSCF level of theory, and the diagonal elements can be energies from CASSCF, MRCI or MRPT2 calculations, *etc.* In particular, MRCI and MRPT2 can include the dynamic correlation that is important in the highly precise electronic structure calculation. Besides, the present work uses the sf-X2C-so-DKH1 Hamiltonian in the BDF package to consider the scalar relativistic effect and the SOC interaction. Due to the 2e-SOC term has been included in the

TABLE 4 Spectroscopy parameters of the $X^2_{3/2}$ and $^2\Pi_{1/2}$ states of AuO

	$X^2\Pi_{3/2}$		$^2\Pi_{1/2}$		
	r_e	ω_e	r_e	ω_e	T_e
CW-icMRCISD+Q	1.867	633	1.889	581	1541
CASPT2[a]	1.861	624	1.884	597	1393
Exp.	1.8487[b]	625[b]	1.917(10)[d]	590(70)[d]	1440±80[d]
	1.9069[c]	646[e]			

[a] Ref. [54].
[b] Ref. [53].
[c] Ref. [51].
[d] Ref. [52].
[e] Ref. [55].

SOC integrals via the molecular mean-field approach, both light and heavy elements can be treated by the present program.

The low-lying states of Halogen and the group IVA atoms are calculated and compared with results from other calculations, verified the validity of our implementation. Our method is superior to those implementations using the BP Hamiltonian, which tends to overestimates the SOC interaction of heavy atoms and also could not be used in the variational calculation. As a pilot application, spectroscopic parameters of two lowest-energy states of AuO are calculated. Our results agree with results calculated on CASPT2 with SOC. Both our and CASPT2 calculations indicate that only full-electron relativistic calculation could produce the reasonable equilibrium bond length of the ground state of AuO. Moreover, our calculation produced a transition energy 1541 cm^{-1} of $X^2\Pi_{3/2} -^2 \Pi_{1/2}$ that is in accordance with the experimental data of 1440 ±80 cm^{-1}.

The work equations used to calculate the SOC matrix elements could extend to the MRCI or MRPT2 wave functions. The Xi'an-CI package implements a flexible internally contracted MRCISD and several MRPT2.[27] All these methods can be used to considering the SOC effects on the SI approach. Furthermore, the variational calculation of SOC is also possible either on the CASSCF level or on the MRCI level. These works are in progress, and we will report our results in the future.

Acknowledgements

B. Suo thanks for the valuable discussion with Prof. Zhendong Li in Beijing Normal University.

Conflict of interest

The authors declare no competing financial interests.

references

[1] Helgaker T, Jørgensen P, Olsen J. Molecular Electronic-Structure Theory. New York: John Wiley & Sons; 2014.

[2] Dyall KG, Fægri Jr K. Introduction to relativistic quantum chemistry. Oxford University Press; 2007.

[3] Szalay PG, Müller T, Gidofalvi G, Lischka H, Shepard R. *Chem. Rev.* **2011**,112,108.

[4] Buenker RJ, Peyerimhoff SD. *J. Chem. Phys.* **1970**,53, 1368.

[5] Werner HJ, Knowles PJ. *J. Chem. Phys.* **1988**, 89, 5803.

[6] Shamasundar K, Knizia G, Werner HJ. *J. Chem. Phys.* **2011**, 135, 054101.

[7] Andersson K, Malqvist PA, Roos BO, Sadlej AJ, Wolinski K. *J. Phys. Chem.* **1990**, 94, 5483.

[8] Andersson K, Malmqvist PA, Roos BO. *J. Chem. Phys.* 1**992**, 96, 1218.

[9] Nakano H. *J. Chem. Phys.* **1993**, 99, 7983.

[10] Lei Y, Liu W, Hoffmann MR. *Mol. Phys.* **2017**, 115, 2696.

[11] Peng D, Liu W, Xiao Y, Cheng L. *J. Chem. Phys.* **2007**, 127, 104106.

[12] Liu W, Peng D. *J. Chem. Phys. 2009*, 131, 031104.

[13] Sikkema J, Visscher L, Saue T, Iliaš M. *J. Chem. Phys. 2009*, 131, 124116.

[14] Liu W. *Natl. Sci. Rev.* **2015**, 3, 204.

[15] Li Z, Xiao Y, Liu W. *J. Chem. Phys.* **2012**, 137, 154114.

[16] Li Z, Xiao Y, Liu W. *J. Chem. Phys.* **2014**, 141, 054111.

[17] Liu W, Hong G, Dai D, Li L, Dolg M. *Theor. Chem. Acc.* **1997**, 96, 75.

[18] Liu W, Wang F, Li L. *J. Theor. Comput. Chem.* **2003**, 2, 257.

[19] Liu W, Wang F, Lemin L. Relativisitic Density Functional Theory: The BDF Program Package. In: Hirao K, Ishikawa Y, editors. Recent advances in relativistic molecular theory Singapore: World Scientific; 2004.p. 257–282.

[20] Zhang Y, Suo B, Wang Z, Zhang N, Li Z, Lei Y, et al. *J. Chem. Phys.* **2020**, 152, 064113.

[21] Cao Z, Li Z, Wang F, Liu W. *Phys. Chem. Chem. Phys.* **2017**, 19, 3713.

[22] Li Z, Suo B, Zhang Y, Xiao Y, Liu W. *Mol. Phys.* **2013**, 111, 3741.

[23] Wang Y, Wen Z, Zhang Z, Du Q. *J. Comput. Chem.* **1992**, 13, 187.

[24] Wang Y, Zhai G, Suo B, Gan Z, Wen Z. *Chem. Phys. Lett.* **2003**, 375, 134.

[25] Suo B, Zhai G, Wang Y, Wen Z, Hu X, Li L. *J. Comput. Chem.* **2005**, 26, 88.

[26] Wang Y, Han H, Lei Y, Suo B, Zhu H, Song Q, et al. *J. Chem. Phys.* **2014**, 141, 164114.

[27] Suo B, Lei Y, Han H, Wang Y. *Mol. Phys.* **2018**, 116, 1051.

[28] Paldus J. *J. Chem. Phys.* **1974**, 61, 5321.

[29] Paldus J. *Phys. Rev. A* **1976**, 14, 1620.

[30] Paldus J. Unitary Group Approach to Many-Electron Correlation Problem. In: Hinze J, editor. The Unitary Group for the evaluation of electronic energy matrix elements Heidelberg: Springer; 1981.p. 1–50.

[31] Shavitt I. *Int. J. Quantum Chem.* **1978**, 14(S12), 5.

[32] Saxe P, Fox DJ, Schaefer III HF, Handy NC. *J. Chem. Phys.* **1982**, 77, 5584.

[33] Gelfand IM, Tsetlin ML. *Dokl. Akad. Nauk. SSSR.* **1950**, 71, 825.

[34] Paldus J. *Int. J. Quantum. Chem.* **1975**, 9(S9), 165.

[35] Wen Z, Wang Y. Theory and Application of Unitary Group Approach. Shanghai, China: Shanghai Scientific and Technical publishers; 1994.

[36] Malmqvist PA, Roos BO, Schimmelpfennig B. *Chem. Phys. Lett.* **2002**, 357, 230.

[37] Fedorov DG, Gordon MS. *J. Chem. Phys.* **2000**, 112, 5611.

[38] Bethe HA, Salpeter EE. Quantum mechanics of one-and two-electron atoms. Springer Science & Business Media; 2012.

[39] Yarkony DR. *Int. Rev. Phys. Chem.* **1992**, 11, 195.

[40] Wen Z, Wang Y, Lin H. *Chem. Phys. Lett.* **1994**, 230, 41.

[41] Celani P, Werner HJ. *J. Chem. Phys.* **2000**, 112, 5546.

[42] Pople J, Seeger R, Krishnan R. *Int. J. Quantum. Chem.* **1977**, 12, 149.

[43] Roos BO, Lindh R, Malmqvist PA, Veryazov V, Widmark PO. *J. Phys. Chem. A* **2005**, 109, 6575.

[44] Veryazov V, Widmark PO, Serrano-Andrés L, Lindh R, Roos BO. *Int. J. Quantum Chem.* **2004**, 100, 626.

[45] Werner HJ, Knowles PJ, Knizia G, Manby FR, Schütz M. *WIREs Comput. Mol. Sci.* 2012, 2, 242.

[46] Berning A, Schweizer M, Werner HJ, Knowles PJ, Palmieri P. *Mol. Phy.* **2000**, 98, 1823.

[47] Barca GMJ, Bertoni C, Carrington L, Datta D, De Silva N, Deustua JE, et al. *J. Chem. Phys.* **2020**, 152, 154102.

[48] Kramida A, Ralchenko Y, Reader J, (2020) NAT;. Accessed: 2021-01-25. NIST Atomic Spectra Database (version 5.8) [Online] `https://physics.nist.gov/asd`.

[49] Mussard B, Sharma S. *J. Chem. Theor. Comput.* **2018**, 14, 154.

[50] Matsunaga N, Koseki S, Gordon MS. *J. Chem. Phys.* **1996**, 104, 7988.

[51] O'Brien LC, Hardimon SC, O'Brien JJ. *J. Phys. Chem. A* **2004**, 108, 11302.

[52] Ichino T, Gianola AJ, Andrews DH, Lineberger WC. *J. Phys. Chem. A* **2004**, 108, 11307.

[53] Okabayashi T, Koto F, Tsukamoto K, Yamazaki E, Tanimoto M. *Chem. Phys. Lett.* **2005**, 403, 223.

[54] O'Brien LC, Oberlink AE, Roos BO. *J. Phys. Chem. A* **2006**, 110, 11954.

[55] Xiang QL, Yang J, Zhang SL, Zhang JC, Ma XW. *Spectrosc. Lett.* 2019, 52, 21.

GRAPHICAL ABSTRACT

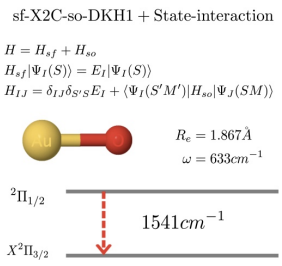

The sf-X2C-so-DKH1 Hamiltonian and state-interaction approach are used to evaluate the spin-orbit coupling on multi-configuration electron correlation theory. The calculated spectroscopic parameters of two lowest states of AuO demonstrate that the present algorithm products the comparable results with the experimental data.